

## Experiments and Kinetic Modeling for the Oxidative Decomposition of Herbaceous and Wooden Residues

Guang-wei Wang,<sup>a</sup> Jian-liang Zhang,<sup>a,\*</sup> Jiu-gang Shao,<sup>b</sup> Yu-kun Jiang,<sup>c</sup> Bin Gao,<sup>a</sup> Di Zhao,<sup>a</sup> Dong-hui Liu,<sup>a</sup> Hai-yang Wang,<sup>a</sup> Zheng-jian Liu,<sup>a</sup> and Ke-xin Jiao<sup>a</sup>

The thermal characteristics of *Paulownia* sawdust (PS), bamboo sawdust (BS), rice lemma (RL), and corncob (CC) in an oxidizing atmosphere were investigated using thermogravimetric analysis. The results indicated that the reaction of biomass oxidative decomposition took place in two main phases: devolatilization and char oxidation. Among various types of biomass, BS was found to possess the highest oxidative decomposition reactivity followed by PS, CC, and RL. Additionally, an increase in heating rate led to a significant improvement of the reactivity. The kinetic modeling of the oxidation reaction with the direct fitting method using the DRPM model showed a satisfied match with the experimental data, and the activation energy of biomass during the devolatilization process was higher than that of the char oxidation process. The activation energy of devolatilization was in the range of 80.7 to 133.8 kJ/mol, while that value of char oxidation fluctuated between 41.7 and 67.5 kJ/mol. In addition, with an increase in the heating rate, a marked compensation effect between the activation energy and pre-exponential factors was observed.

*Keywords:* Biomass; Thermogravimetric analysis; Oxidation; Kinetics model

*Contact information:* a: School of Metallurgical and Ecological Engineering, University of Science and Technology Beijing, Beijing 100083, China; b: Handan Steel Co., Ltd., Handan, 056000, China; c: School of Materials Science and Engineering, University of Science and Technology Beijing, Beijing 100083, China; \*Corresponding author: zhang.jianliang@hotmail.com

### INTRODUCTION

In recent years, China has made great progress in developing its economy, which inevitably led to increased energy consumption and CO<sub>2</sub> emission. According to the China energy statistical yearbook (NBS 2014), the energy consumption per unit GDP is 4 to 5 times higher than that of some developed countries, and its CO<sub>2</sub> emission is even over 5 to 6 times higher. China mainly consumes coal (approximately 66%), petroleum, and natural gas (Yu and Kong 2013; NBS 2014; Zhu and Luo 2015). Therefore, in the Outline of the China's 12<sup>th</sup> Five-Year Economic and Social Development Plan (NDRC 2010), the government has made it clear that the energy structure should be changed from mainly relying on coal to the use of green and diverse, low-carbon energy sources for the implementation of sustainable economic and social development. Compared with fossil fuels such as traditional coal, agricultural and forestry residue is one type of high-capacity, widespread, and renewable source of clean energy. Since it does not cause CO<sub>2</sub> emissions, the use of agricultural and forestry residue could slow down the increasingly severe global greenhouse effect (Azar *et al.* 2006; Lehmann 2007). Known as an abundant agricultural residue, straw and stalk residue as an energy source is equivalent to 480 million tons of standard coal (Zhao and Wang 2008; Wang *et al.* 2010). Straw used to be a main source of

fuel in rural areas. However, because of the widespread use of coal, oil, gas, electricity, and other commercial energies, most biomass residue is directly burned, causing waste and air pollution. Therefore, new technologies should be explored in order to use biomass effectively, which can greatly accelerate the energy modernization of rural residents and thus meet the urgent demand for high-quality energy. Additionally, the use of these residues could reduce the harmful effects of burning on the environment and society, realizing the efficient utilization of residues (Norgate *et al.* 2012).

Currently, agricultural and forestry residues have been applied in many fashions, such as fermentation, gasification, direct combustion, and power generation (Cheng *et al.* 2012; Sait *et al.* 2012; Amutio *et al.* 2013; Ceylan *et al.* 2014). Much attention has been concentrated on the combustion of herbaceous (relating to one type of plant that has a soft stem, such as rice, corn, cotton, wheat, *etc.*) and wooden (a plant having hard lignified tissues or woody parts especially stems, such as pine, tung, aspen, cypress, *etc.*) residue owing to its economical convenience, high production, and high adaptability (Chen *et al.* 2011). Wang *et al.* (2013) investigated the combustion characteristics of seaweed using a small fluid bed device and studied the release process of NO<sub>x</sub>, SO<sub>2</sub>, and CO.

By analyzing the composition of litter straw, rice straw, corn stalk, and corncob, Zhu *et al.* (2006) concluded that hemicellulose is easy to pyrolyze, while cellulose and lignin are more difficult to pyrolyze. Furthermore, the main pyrolysis product of hemicelluloses and cellulose is volatile, but the product of lignin is char. Li *et al.* (2012) investigated the effect of oxygen concentration in an oxidizer on the ignition of biogas. The ignition process was investigated through a closed homogeneous reactor model of CHEMKIN4.0 code, and a sensitivity analysis was conducted at the same time.

All of the aforementioned research was focused on the oxidation decomposition characteristics of biomass, but little attention was paid to the kinetics of the biomass oxidation decomposition. The combustion kinetics of biomass samples focuses on the effect of temperature, time, and other factors on the reaction conversion during the combustion process. An analysis of combustion kinetics could elucidate the mechanism of biomass combustion, further predict the reaction process, and improve the effective utilization rate.

Amutio *et al.* (2012; 2013) further studied the oxidation and combustion of biomass by setting up six homogeneous reaction dynamics that were well-fitting to the biomass of the combustion process including the decomposition of hemicelluloses, cellulose, and lignin, as well as the combustion of residual carbon. However, the calculation process is very complicated, and the assumptions of homogeneous reactions applied for all components of the combustion process need further analysis.

In this study, the oxidative decomposition of four different types of biomass—*Paulownia* sawdust, bamboo sawdust, rice lemma, and corncob (four types of the most commonly seen agricultural and forestry residues with an abundant production every year in Henan province, China)—were studied at different heating rates using the thermogravimetric analysis. A double parallel reaction random pore model based on a traditional gas-solid reaction random pore model was built. The kinetic parameters of the oxidative decomposition process for different types of biomass were calculated using the nonlinear fitting method. This article offers a theoretical basis for optimizing the design of the biomass boiler as well as expanding the use of biomass in power plants and steel plants.

## EXPERIMENTAL

### Materials

Two wooden residues including *Paulownia* sawdust (PS), bamboo sawdust (BS), as well as two herbaceous residues including rice lemma (RL), and corncob (CC) were collected from Yuzhou city, Henan province, China. The samples were ground and sieved to a < 0.074-mm particle size and oven-dried for 24 h at 105 °C. After drying, the samples were stored in sealed containers. The characteristic values of the raw materials are given in Table 1. The proximate and ultimate analysis results of the raw materials were conducted according to the Chinese standards GB/T 212-2001 (2001) and GB/T 476-2001 (2001), respectively. The gross calorific value of the raw materials was determined using an IKAC-2000 calorimeter (IKA Works Guangzhou, Guangzhou, China) basic value of samples according to ASTM D240-02 (2007). The ash content was determined by combusting the samples at 800 °C, and the compositional analysis of ash is listed in Table 2.

**Table 1.** Proximate and Ultimate Analysis of Samples

Sample	Proximate Analysis (wt.%)			Ultimate Analysis (wt.%)					HHV (MJ/kg)
	FC <sub>d</sub> <sup>a</sup>	A <sub>d</sub>	V <sub>d</sub>	C <sub>d</sub>	H <sub>d</sub>	O <sub>d</sub> <sup>a</sup>	N <sub>d</sub>	S <sub>d</sub>	
PS	21.67	5.82	72.51	46.18	5.97	43.78	0.32	0.07	18.43
BS	22.49	2.98	74.53	51.25	2.91	39.16	0.29	0.09	17.17
RL	16.17	17.13	66.71	40.78	5.17	37.05	0.28	0.04	16.48
CC	17.82	1.98	80.23	45.33	3.70	43.31	0.46	0.14	15.86

<sup>a</sup> Calculated by difference. FC, fixed carbon content; A, ash content; V, volatile matter content; d, dry basis; HHV, high calorific value

**Table 2.** Composition Analysis of Ash in Biomass

Sample	SiO <sub>2</sub>	Al <sub>2</sub> O <sub>3</sub>	Fe <sub>2</sub> O <sub>3</sub>	CaO	Na <sub>2</sub> O	K <sub>2</sub> O	MgO
PS	36.30	3.52	4.11	21.39	3.40	12.32	9.29
BS	9.41	0.50	2.52	4.04	0.16	61.59	2.64
RL	81.03	0.76	4.69	2.32	0.52	7.06	0.58
CC	28.87	1.89	3.14	3.56	0.79	47.43	1.21

### Thermogravimetric Analysis

Oxidative decomposition characteristics of different types of the biomass were determined using a thermogravimetric analyzer (HCT-3, Henven Scientific Instrument Factory, Beijing, China) under an air atmosphere. The flow rate of air was 100 mL/min. Approximately 5 mg of sample was heated from room temperature up to 750 °C at various heating rates (2.5, 5, 10, and 20 °C/min). A small amount of sample together with slow heating rates was used for the purpose of avoiding heat transfer limitations and minimizing mass transfer effects. Before the start of the experiment, several experiments without samples were carried out to obtain the baseline, which was deducted when the experiments with samples started, in order to eliminate the systematic error of the instrument itself. To reduce the experimental error as much as possible, all tests at a given heating rate were performed in triplicate, and the reproducibility was quite high.

The oxidative decomposition fractional conversion ( $x$ ) was calculated using the following equation:

$$x = \frac{(m_0 - m_t)}{(m_0 - m_{\text{ash}})} \quad (1)$$

where  $m_0$  denotes the sample mass at the start of oxidative decomposition,  $m_t$  the mass of the sample at oxidative decomposition time  $t$ , and  $m_{\text{ash}}$  the mass of ash remaining in the sample after its conversion was completed.

## RESULTS AND DISCUSSION

### Thermogravimetric Characteristics

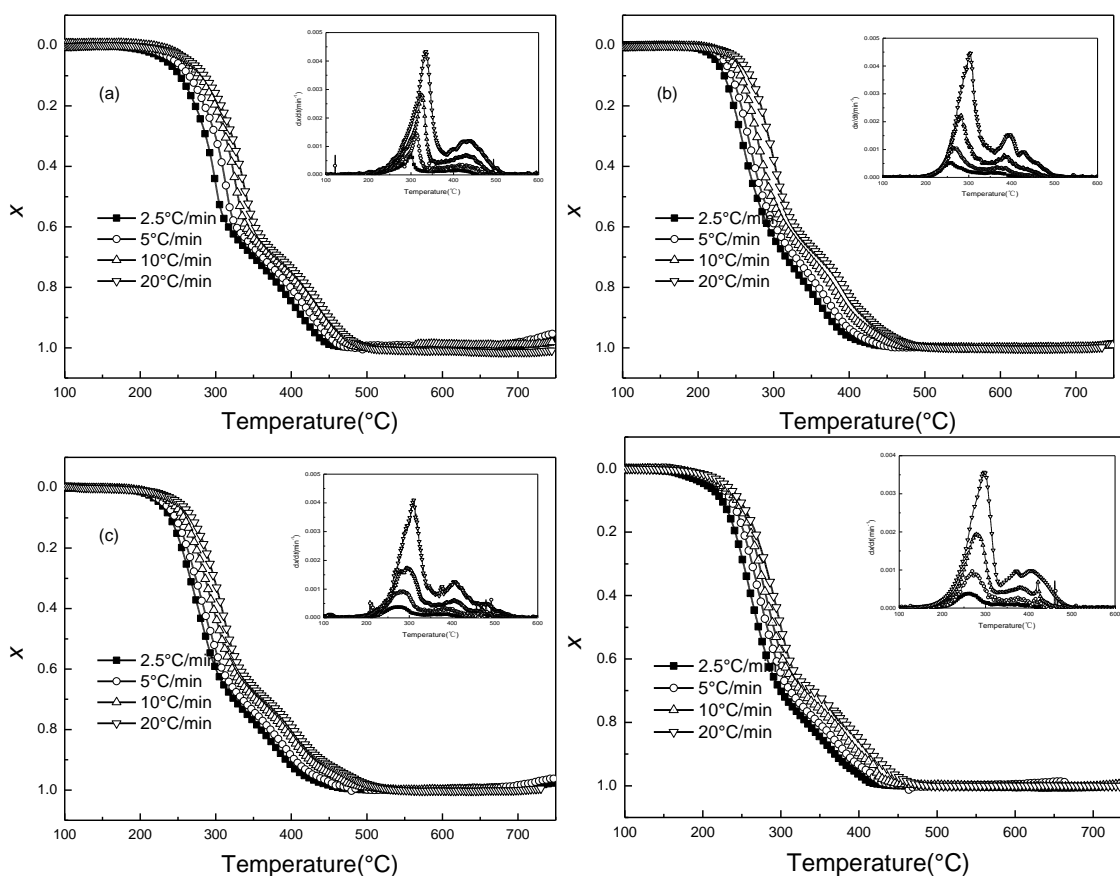


**Fig. 1.** Experimental fractional conversion and reaction rate curves of the four types of biomass: (a) PS, (b) BS, (c) RL, and (d) CC

Figure 1 presents the fractional conversion and reaction rate curves of different biomass samples at different heating rates. All reaction curves exhibited one common characteristic: they all had two weight loss platforms as shown by the reaction rate curves, and two main peaks were readily distinguished. The reaction of oxidative decomposition was divided into two individual stages. The range of the first stage was from 200 to 300 °C, which represented pyrolysis and heterogeneous oxidation. In contrast, the second stage (300 to 480 °C), where the peak in the reaction rate curve was low and broad, represented the combustion of char formed after the first stage. Meanwhile, the mass loss rate of the

first stage was approximately 60%, with a maximum weight loss rate peak far higher than that of the second stage. This result reflects that biomass contains hemicelluloses, cellulose, lignin, *etc.*, and the carbon-carbon bond of carbonaceous, semi-volatile components or a congregation of organic matters joined together that existed in cells rupture to produce CO<sub>2</sub>, CO, and part of the water vapor leading to mass loss (Hu *et al.* 2015). The mass loss rate of the second stage was approximately 40%, but the proximate analysis of biomass showed that the fixed carbon content was approximately 20%, which was significantly less than the mass loss of the second stage. Thus, the mass loss of biomass at this stage was not only caused by the combustion of a small amount of fixed carbon, but also by the combustion of organic compounds with high boiling points, such as lignin.

For a comprehensive analysis of the oxidative decomposition characteristics of the four types of biomass residue, parameters including ignition temperature ( $T_i$ ), burnout temperature ( $T_f$ ), peak temperature ( $T_p$ ), and combustion characteristic index ( $S$ ) were calculated from the TG/DTG curves (Li *et al.* 2006; Wang *et al.* 2014; Wang *et al.* 2015).  $T_i$  was determined based on the temperature at which the DTG had its peak value and the corresponding slope to the intersection with respect to the TG profile.  $T_f$  is the temperature at which the rate of weight loss becomes smaller than  $0.0001 \text{ s}^{-1}$ .  $T_p$  describes the corresponding temperature of the rate of weight loss at the profile peak.  $S$  is the comprehensive characteristic index, defined in Eq. 2 as,

$$S = \frac{(\text{dx/dt})_{\text{max}} \cdot (\text{dx/dt})_{\text{mean}}}{T_i^2 \cdot T_f} \quad (2)$$

where  $(\text{dx/dt})_{\text{max}}$  and  $(\text{dx/dt})_{\text{mean}}$  are the maximum mass loss rate and average mass loss rate, respectively. The average reaction rate refers to the weighted average of the instantaneous reaction rate at temperatures ranging from  $T_i$  to  $T_f$ .

The oxidative decomposition parameters are listed in Table 3. In an ascending order, the  $T_i$  values were CC, BS, RL, and PS, and the  $T_f$  values were BS, CC, RL, and PS. At a heating rate of  $10 \text{ }^\circ\text{C/min}$ , the  $T_i$  and  $T_f$  values of CC, BS, RL, and PS were 215.4, 242.8, 249.9, 272.1, and 463.5, 465.6, 486.3, and 489.9  $^\circ\text{C}$ , respectively. The peak value of the two combustive stages was different. At  $10 \text{ }^\circ\text{C/min}$ ,  $\text{dx/dt}_{\text{max-1}}$  in the first stage was ranked as  $\text{PS} > \text{BS} > \text{CC} > \text{RL}$ ;  $\text{dx/dt}_{\text{max-2}}$  in the second stage and  $\text{dx/dt}_{\text{mean}}$  were both ordered as  $\text{BS} > \text{CC} > \text{PS} > \text{RL}$ . Comparing all of the above results, none of the parameters ( $T_i$ ,  $T_f$ ,  $\text{dx/dt}_{\text{max-1}}$ ,  $\text{dx/dt}_{\text{max-2}}$ , and  $\text{dx/dt}_{\text{mean}}$ ) had the same rule, and so only one characteristic parameter cannot represent the reaction reactivity of biomass. Thus, the comprehensive characteristic index ( $S$ ) as reported by Li *et al.* (2011) was used to represent the oxidative decomposition reactivity of different biomass samples. The  $S$  values of different samples from high to low were ranked as BS, PS, CC, and RL.

Previous research suggested that alkali metal oxides in biomass had obvious catalytic effects on the decomposition of volatiles and the combustion of char (Jenkins *et al.* 1998; Huang *et al.* 2009; Lahijani *et al.* 2013a). Tables 1 and 2 show the proximate and ash analysis results of the four different biomasses. The content of alkali and alkaline-earth metal oxides (K, Na, and Ca) in BS and PS were higher than those in CC and RL. K, Na, and Ca generally act as catalysts to prompt the combustion. The order of the catalytic index was  $\text{BS} > \text{PS} > \text{CC} > \text{RL}$ , and further results suggested that the combustion reactivity of biomass was mainly related to the mineral contents.

**Table 3.** Characteristic Oxidative Decomposition Parameters of Biomass at Different Heating Rates

Sample	Heating Rate (°C/min)	$T_i$ (°C)	$T_{p-1}$ (°C)	$dx/dt_{max-1}$ (min <sup>-1</sup> )	$T_{p-2}$ (°C)	$dx/dt_{max-2}$ (min <sup>-1</sup> )	$T_f$ (°C)	$dx/dt_{mean}$ (min <sup>-1</sup> )	$S \times 10^{15}$	$t_c$ (min)
PS	2.5	243.2	299.1	7.04E-04	410.5	1.53E-04	440.5	1.69E-04	0.63	78.92
	5	256.4	311.2	1.44E-03	421.4	3.16E-04	465.9	3.32E-04	2.31	41.90
	10	272.1	324.4	2.79E-03	431.6	6.71E-04	489.9	7.85E-04	9.66	21.78
	20	276.2	332.8	4.33E-03	434.5	1.22E-03	512.7	1.54E-03	28.13	11.83
BS	2.5	223.4	258.8	4.93E-04	361.2	1.70E-04	391.3	2.58E-04	0.78	67.16
	5	231.7	267.9	1.04E-03	373.8	3.40E-04	427.9	4.21E-04	2.45	39.24
	10	242.8	280.5	2.42E-03	383.6	7.69E-04	463.5	8.51E-04	10.51	22.07
	20	256.6	301.5	4.44E-03	397.2	1.53E-03	496.6	1.63E-03	33.53	12.00
RL	2.5	225.8	273.5	4.07E-04	377.9	1.40E-04	441.2	2.43E-04	0.56	86.16
	5	234.7	284.8	9.53E-04	392.8	3.01E-04	460.6	4.12E-04	2.08	45.18
	10	249.9	294.7	1.78E-03	403.6	6.03E-04	486.3	7.22E-04	6.19	23.64
	20	253.2	308.9	4.12E-03	407.5	1.23E-03	509.6	1.53E-03	27.19	12.82
CC	2.5	201.2	258.8	3.92E-04	360.6	1.26E-04	400.8	2.11E-04	0.55	79.84
	5	216.1	273.8	9.75E-04	374.9	2.75E-04	430.9	4.04E-04	2.34	42.96
	10	215.4	281.6	1.95E-03	383.4	5.37E-04	465.6	8.24E-04	9.12	25.02
	20	217.3	296.8	3.55E-03	388.1	1.02E-03	496.9	1.62E-03	31.1	14.98

Notes:  $T_i$ , ignition temperature;  $T_{p-1}$ , corresponding temperature of the first peak;  $T_{p-2}$ , corresponding temperature of the second peak;  $T_f$ , burnout temperature;  $(dx/dt)_{max-1}$ , value of the first peak;  $(dx/dt)_{max-2}$ , value of the second peak;  $(dx/dt)_{mean}$ , mean reaction rate;  $S$ , combustion characteristic index;  $t_c$ , time zone

With increasing heating rates,  $T_i$ ,  $T_f$ ,  $T_{p-1}$ , and  $T_{p-2}$  were increased, and fractional conversion curves also moved to a high temperature range. The same phenomenon was observed in a previous research on biomass char gasification (Wang *et al.* 2015). It may be explained that the thermal decomposition under high heating rate was affected by the rate of heat transfer inside the biomass materials as a result of the steep temperature gradient between the biomass particles and the surrounding. With an increased heating rate, the  $dx/dt_{max}$ ,  $dx/dt_{mean}$ , and  $S$  values all increased because it provided a higher thermal energy to facilitate better heat transfer between the surrounding and inside the samples. Meanwhile, the time needed for oxidative decomposition ( $t_c$ ) was shortened. For example, as the heating rate increased from 2.5 °C/min to 20 °C/min, the index ( $S$ ) of BS increased from  $0.78 \times 10^{-15}$  to  $33.53 \times 10^{-15}$ , while the  $t_c$  was shortened from 67.16 min to 12.00 min. Therefore, the reactivity of biomass was improved due to an increase in the heating rate.

### Kinetic Models

Kinetic data from a solid-state reaction was obtained using thermogravimetric analysis. The oxidative decomposition curve is usually derived as a sum of the corresponding individual component contributions (Heikkinen *et al.* 2004; Gil *et al.* 2010). As shown in Fig. 2, the kinetic pathway of oxidation results from two competitive processes: particle ignition dominated by either burning volatile matter (reactions A and B) or heterogeneous combustion (reaction C) (Senneca *et al.* 2002; Amutio *et al.* 2012).

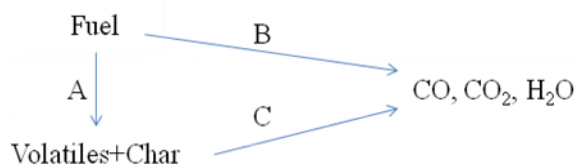


**Fig. 2.** Possible mechanisms for solid conversion in an oxidative atmosphere

The kinetic model proposed in this work is similar to that described in a previous report for the determination of the combustion kinetic parameters of coal/biomass blends (Wang *et al.* 2014). The model corresponds to a multi-component mechanism, in which the oxidative decomposition takes place in two stages: (1) pyrolysis and heterogeneous oxidation; and (2) char combustion. Oxidative decomposition is assumed to contain two parallel reactions that occur simultaneously, as indicated by Font *et al.* (1991). The overall reaction and the two individual reactions are expressed by Eqs. 3, 4, and 5, respectively. Each component decomposes simultaneously at different rates and temperatures. In addition, if the mass transfer resistance through an external fluid film and within the porous particle is neglected, the overall rate of a gas-solid reaction is completely controlled by the chemical reactivity of the surface.



The overall reaction rate of biomass oxidation is described by Eq. 6:

$$\frac{dx}{dt} = \sum_{i=1}^2 c_i k_i (P_g, T) \frac{S(x_i)}{S_0} \quad (6)$$

In this case,  $S(x_i)/S_0$  describes the relative change in available surface area during the reaction. Several models have been developed for the structural function of  $S(x_i)/S_0$ , and the most commonly used are the grain model (GM) and the random pore model (RPM). The random pore model developed by Bhatia and Perlmutter (1980) is more advantageous than the grain model for modeling the combustion of both coal and biomass (Wang *et al.* 2014; Zhang *et al.* 2014). Using the RPM, the reaction rate of char is denoted in Eq. 7,

$$\frac{dx}{dt} = \sum_{i=1}^2 c_i k_{0-i} e^{-\frac{E_i}{RT}} (1-x_i) \sqrt{1-\psi_i \ln(1-x_i)} \quad (7)$$

where  $k_{0-i}$  and  $E_i$  are the pre-exponential factor and activation energy corresponding to the mass loss of the  $i$  pseudo component, respectively,  $x_i$  is the fractional conversion at the time ( $t$ ) of each pseudo component, and  $c_i$  is the mass concentration of volatiles and char in each type of biomass material. As the values of  $c_i$  are unknown for these types of biomass materials, they also were calculated.

In this study, the modified RPM shown in Eq. 7 is defined as the double-parallel-random pore model (DRPM). Given that the runs followed a temperature ramp, the pre-exponential kinetic parameter,  $k_{0-i}$ , and activation energy,  $E_i$ , were calculated by fitting the experimental results obtained by deconvolution to Eq. 7 integrated for each pseudo component. The nonlinear least-squares fitting method was employed to obtain the kinetic parameters, and the objective function can be written as Eq. 8,

$$OF = \sum_{i=1}^N \left( \left( \frac{dx}{dt} \right)_{\text{exp},i} - \left( \frac{dx}{dt} \right)_{\text{calc},i} \right)^2 \quad (8)$$

where  $\left( \frac{dx}{dt} \right)_{\text{exp},i}$  represents the experimental data,  $\left( \frac{dx}{dt} \right)_{\text{calc},i}$  is the value calculated by the model, and  $N$  is the number of experimental data available.

Under the temperature-programmed reaction conditions, the heating rate in the oxidative decomposition of biomass is  $\beta$ . Therefore, the relationship between reaction temperature ( $T$ ) and combustion time ( $t$ ) is shown in Eq. 9,

$$T = T_0 + \beta t \quad (9)$$

where  $T_0$  is the starting temperature of 298 K.

Equations 7 and 9 can be integrated to give Eq. 10,

$$x = \sum_{i=1}^2 c_i \cdot \left( 1 - \exp \left( - \left( k_{0-i} \cdot \frac{(T-T_0)}{\beta} \cdot \exp \left( \frac{-E_i}{RT} \right) \right) \cdot \left( 1 + \frac{k_{0-i} \cdot \psi}{4} \cdot \frac{(T-T_0)}{\beta} \cdot \exp \left( \frac{-E_i}{RT} \right) \right) \right) \right) \quad (10)$$

where  $\psi$  is the parameter of the particle structure, whose format is

$$\psi = \frac{4\pi L_0 (1-\varepsilon_0)}{S_0^2} \quad (11)$$

where  $S_0$  is the pore surface area,  $L_0$  is the pore length, and  $\varepsilon_0$  is the particle porosity.

Equation 10 is used to calculate  $x$  using the previously estimated  $k_0$  and  $E$ . The calculation of  $x$  was performed in order to verify the reliability of the kinetic model and its capacity to describe not only the reaction rate ( $dx/dt$ ) but also the fractional conversion ( $x$ ).

During model building, some assumptions and simplifications were made for the gas-solid reaction. However, the actual oxidative decomposition process is far more complicated, so the model should be validated by calculating the error between experimental and calculated data. By comparing these two experimental and fitted  $dx/dt$  and  $x$  values, the errors between the experimental and calculated data were calculated using Eqs. 12 and 13:

$$DEV\left(\frac{dx}{dt}\right)(\%) = 100 \times \frac{\left(\sum_{i=1}^N \left(\frac{dx}{dt}_{\text{exp},i} - \frac{dx}{dt}_{\text{calc},i}\right)^2 / N\right)^{1/2}}{\max\left(\frac{dx}{dt}\right)_{\text{exp}}} \quad (12)$$

$$DEV(x)(\%) = 100 \times \frac{\left(\sum_{i=1}^N (x_{\text{exp},i} - x_{\text{calc},i})^2 / N\right)^{1/2}}{\max(x)_{\text{exp}}} \quad (13)$$

where  $DEV\left(\frac{dx}{dt}\right)(\%)$  and  $DEV(x)(\%)$  are the relative error margins,  $\frac{dx}{dt}_{\text{exp},i}$  and  $x_{\text{exp},i}$  are experimental values,  $\frac{dx}{dt}_{\text{calc},i}$  and  $x_{\text{calc},i}$  are calculated values,  $\max\left(\frac{dx}{dt}\right)_{\text{exp}}$  and  $\max(x)_{\text{exp}}$  are the experimental maximum reaction rate and fraction conversion, respectively, and  $N$  is the amount of points taken by the experimental data.

### Kinetic Parameters

All kinetic parameters were calculated using the DRPM model (Table 4), and the experimental and calculated data were compared in Fig. 3. The experimental and calculation reaction rate curves of CC fit best, followed by RL. BS and PS were worse, as demonstrated by the correlation coefficient  $R^2$  in Table 4. This result may indicate alkali and alkaline-earth metal oxides (K, Na, and Ca) in the biomass, which have strongly catalytic effects on oxidative decomposition. The RPM model is based on the hypothesis of the non-catalytic gas-solid reaction, and it only reflects the change of the reaction area along with fractional conversion, without considering the effects of the number of active sites on the reaction surface on the process of oxidation. However, alkali and alkaline-earth metal oxides (K, Na, and Ca) are able to change the distribution and density of active sites on the reaction surface, resulting in the calculated values being lower than the experimental values. In this study, the two wooden residues had more K, Na, Ca-alkali, and alkaline-earth metal oxides than the herbaceous residues, which explains why the former fitting result was lower than the latter, as previously described (Lahijani *et al.* 2013b; Zhang *et al.* 2014).

As shown in Table 4, the first stage corresponding to the volatile content released from BS, RL, and CC was reduced, and the percentage of residual carbon combustion increased when heating rates increased, which can be ascribed to there being insufficient time for volatile materials to release and combust before the combustion of residual char began. At the same time, the main components (cellulose, lignin, and hemi-cellulose) of biomass are comprised of similar but different units connected by bridged bonds. These units contain a condensate aromatic nucleus with a variety of functional groups.

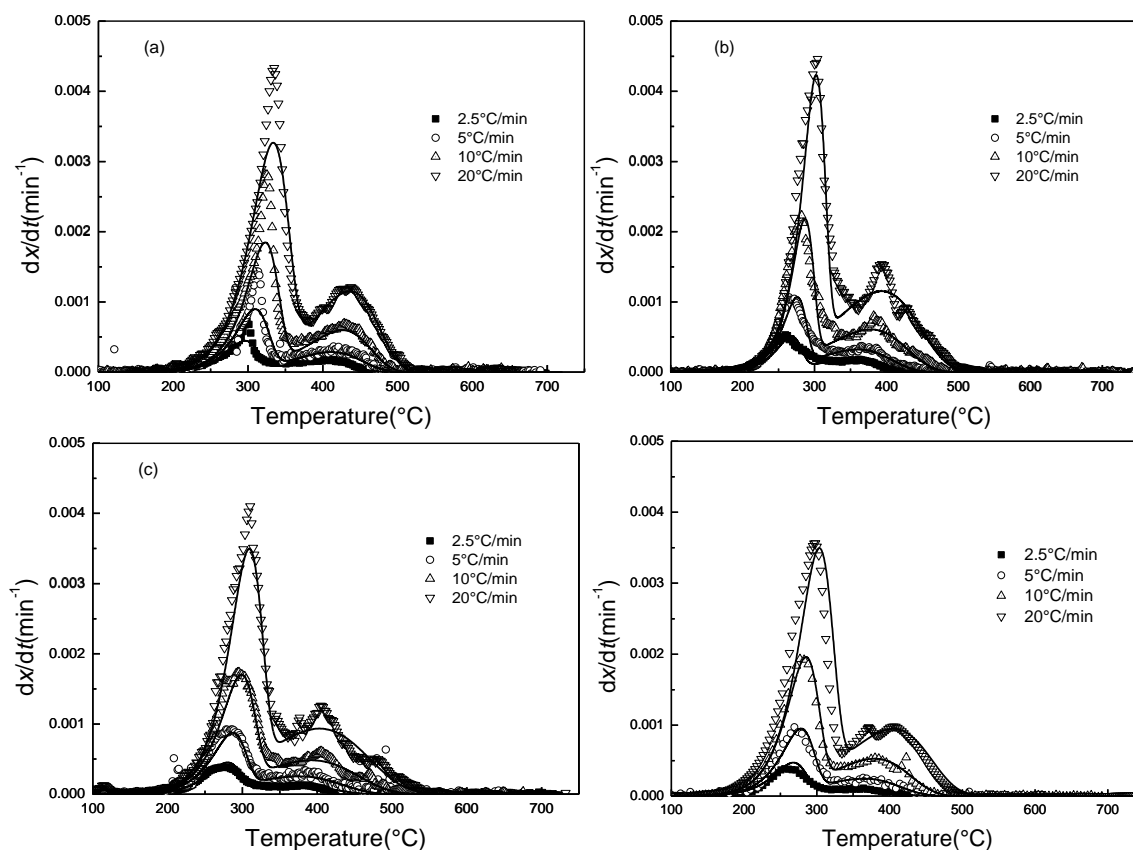


**Fig. 3.** Experimental reaction rate curves of biomass samples and fitting curves: (a) PS; (b) BS; (c) RL; and (d) CC

Parts of the aromatic nucleus have a high thermal stability, but the active functional groups have poor thermal stability. When heated, the functional groups are easily cracked and released, but the aromatic nucleus is difficult to destroy. Furthermore, with a higher heating rate, there was a sufficiently high thermal shock to destroy the stability of the condensate aromatic nucleus. The release of volatile matter was prolonged, resulting in increased final volatile composition. This may explain why the volatile content released from PS increased with increased heating rates.

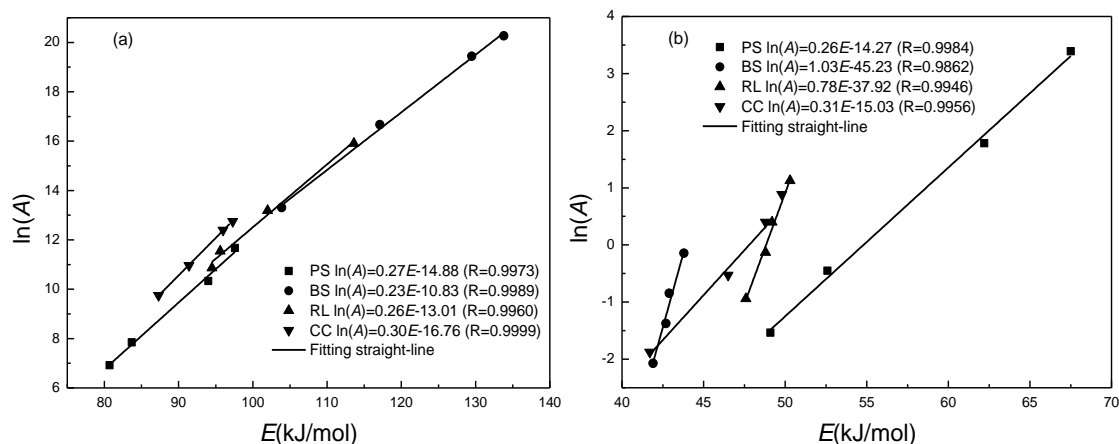
At the same heating rate, the rate of volatile oxidation was in the following order: BS > RL > CC > PS, and in the residual char combustion stage the volatile oxidation rate was PS > RL > CC > BS. The activation energy of the first stage was larger than that of the second one. Xu *et al.* (2010) and Wang *et al.* (2014) observed the same phenomenon, and there are three aspects that explain the above situation. First, in the low temperature region, more energy is needed to maintain the combustion reaction. The combustion reaction of residual char mainly occurs in the high temperature region; however, it consumes a smaller amount of energy. Secondly, one consequence of the transient nature of non-isothermal experiments is that the physical structure of the sample is continuously changing during the reaction.

Volatile matter was initially released in the low temperature range, and at this time, residual char was preheated but not ignited. Only after the temperature of residue char reached ignition was there release of a large amount of heat.

**Table 4.** Kinetic Parameters of the Biomass Samples during Oxidative Decomposition at Four Heating Rates

Samples	Heating Rate (°C/min)	$c_1$	$E$ (kJ/mol)	$k_0$ (min <sup>-1</sup> )	$\psi_1$	$c_2$	$E$ (kJ/mol)	$k_0$ (min <sup>-1</sup> )	$\psi_2$	$R^2$
PS	2.5	0.5639	80.7	1.01E+03	7.01	0.4361	49.1	2.15E-01	7.49	0.9985
	5	0.5808	83.7	2.56E+03	6.62	0.4192	52.6	6.36E-01	7.66	0.9986
	10	0.5951	94.0	3.06E+04	4.44	0.4049	62.2	5.92	5.64	0.9991
	20	0.5963	97.6	1.17E+05	1.40	0.4037	67.5	2.97E+01	2.87	0.9993
BS	2.5	0.4842	103.9	6.01E+05	2.78	0.5158	41.9	1.26E-01	5.57	0.9995
	5	0.4786	117.1	1.73E+07	2.46	0.5214	42.7	2.53E-01	4.76	0.9992
	10	0.4731	129.5	2.78E+08	2.27	0.5269	42.9	4.29E-01	4.00	0.9996
	20	0.4710	133.8	6.31E+08	2.04	0.5290	43.8	8.65E-01	3.14	0.9994
RL	2.5	0.5339	94.5	5.20E+04	1.12	0.4661	47.6	3.91E-01	1.50	0.9994
	5	0.5252	95.6	1.03E+05	0.80	0.4748	48.8	8.77E-01	1.39	0.9996
	10	0.5168	102.0	5.35E+05	0.58	0.4832	49.2	1.49	1.07	0.9998
	20	0.5118	113.6	8.10E+06	0.38	0.4882	50.3	3.08	0.81	0.9997
CC	2.5	0.5871	87.3	1.72E+04	1.64	0.4129	41.7	1.53E-01	2.38	0.9998
	5	0.5817	91.4	5.78E+04	1.51	0.4183	46.5	5.90E-01	2.13	0.9997
	10	0.5765	96.0	2.41E+05	1.37	0.4235	48.8	1.49	1.97	0.9998
	20	0.5648	96.8	3.45E+05	1.36	0.4352	49.8	2.42	0.51	0.9996

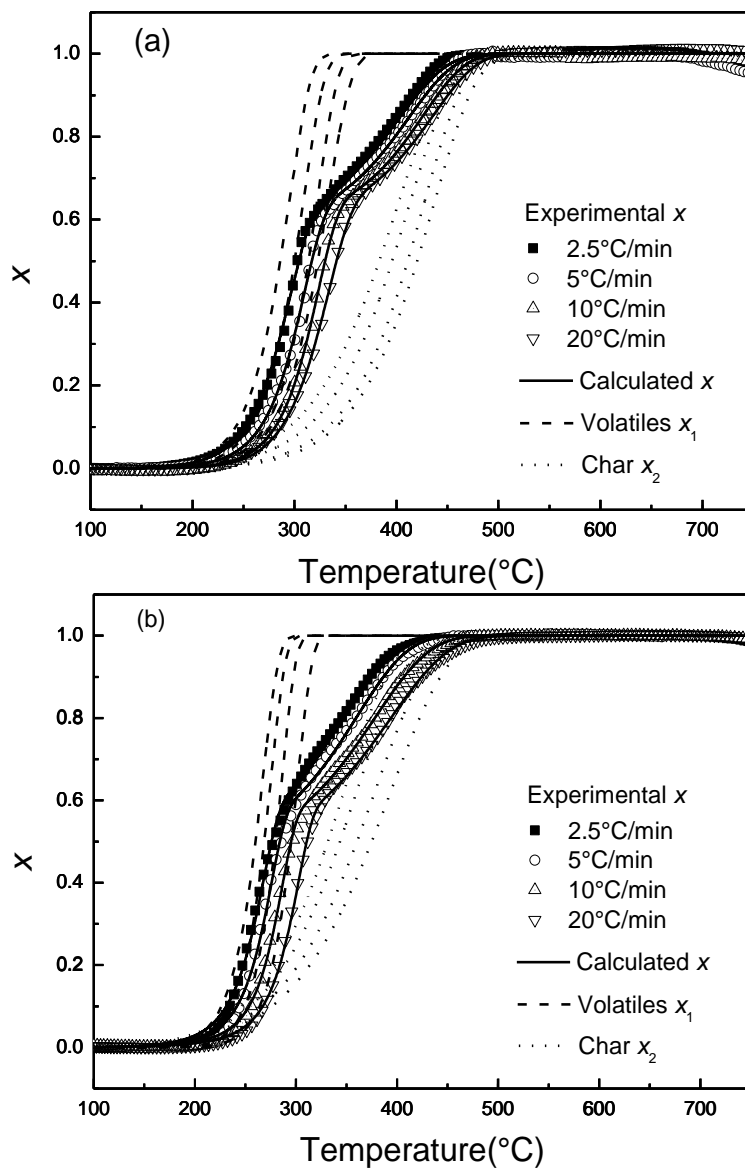
Because the influence of temperature on the interfacial chemical rate constants and diffusion rate constants is different, the controlled step of oxidative decomposition was changed from chemical reaction to diffusion with increasing temperature. Generally speaking, the activation energy of the reaction in the diffusion control was smaller than that of the chemical reaction control. As combustion proceeded, carbon was continuously removed, thereby opening the pore and reducing diffusion resistance. The  $\psi$  value of the residue char combustion stage was higher than that of the volatile oxidation. Finally, a progressive conversion mode of the oxidation may also become dominant, thereby enlarging the fraction of the particle actually available to reaction. Those effects enhance the reaction rate and contribute to a decrease in activation energy. In this study, the activation energies of the first stage lie in the range of 80.7-133.8kJ/mol, and in the second stage which is between 41.7kJ/mol and 67.5kJ/mol. In a previous study, Shen *et al.* (2009) calculated first stage activation energy value for pine, aspens, birch, and oak in air atmosphere in the range between 114kJ/mol and 119kJ/mol. Some researchers (Sun *et al.* 2010) obtained activation energy values for cotton stalk under air atmosphere of 108 kJ/mol. Liu *et al.* (2015a) indicated that the second stage activation energies of beetroot and switchgrass in the range of 38.06 kJ/mol to 71.36 kJ/mol. Activation energies reported in literature are similar with the results in this study.



**Fig. 4.** Relationship between  $\ln A$  and  $E$ . (a) Oxidation of volatile matter; (b) combustion of residual carbon

The activation energies for the first and second stage for all samples differed from each other (Table 4). The activation energy increased with increasing heating rate. For example, the activation energy value for PS in the first stage was 80.7 kJ/mol at 2.5 °C/min, 83.7 kJ/mol at 5 °C/min, 94.0 kJ/mol at 10 °C/min, and 97.6 kJ/mol at 20 °C/min, while in the second stage it was 49.1 kJ/mol at 2.5 °C/min, 52.6 kJ/mol at 5 °C/min, 62.2 kJ/mol at 10 °C/min, and 67.5 kJ/mol at 20 °C/min. The heating rate influences the temperature ranges of the oxidative decomposition process, which causes spatial gradients of temperature or significant differences in temperature between the controlling thermocouple and the sample, especially when a poor contact between the thermocouple and sample is present. At the same time, the pre-exponential factors of both stages increased with increasing heating rate. At different heating rates, there was an obvious linear relationship between  $E$  and  $\ln A$ , which is defined as the kinetic compensation effect in the dynamic analysis (Fig. 6). These phenomena were also observed in biomass pyrolysis, biomass/coal

blends combustion, and the pyrolysis and combustion characteristics of coal (White *et al.* 2011; Wang *et al.* 2012; Liu *et al.* 2015b). Thus, the model has an obvious kinetic compensation effect, which also establishes the validity of the model in describing complicated combustion processes.



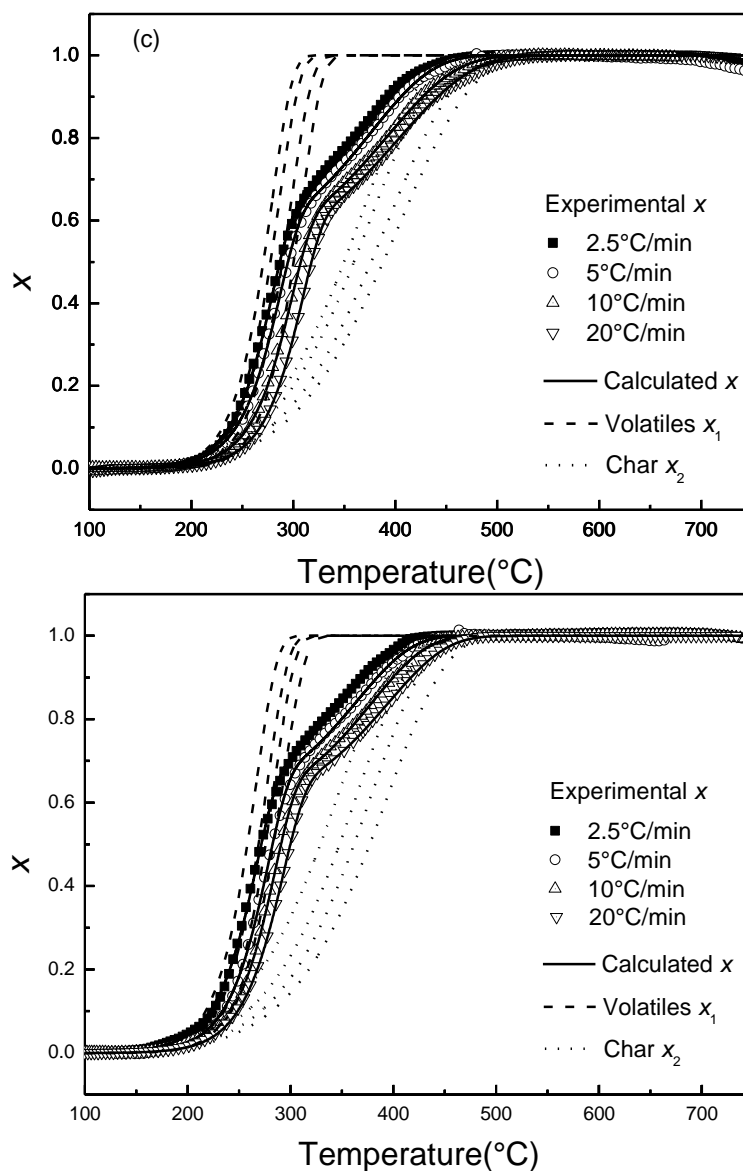


**Fig. 5.** Experimental fractional conversion curves of biomass and those calculated from a model using parameters determined from different heating rates: (a) PS; (b) BS; (c) RL; and (d) CC

To further show the fitted reliability in this research, the oxidation fractional conversion curves of the biomass were further calculated from the kinetic parameters as listed in Table 4 using Eq. 9, and the results are shown in Fig. 5. The dotted lines represent the fractional conversion curves of volatile oxidation (line  $x_1$ ) and residual char combustion (line  $x_2$ ). Furthermore, the solid line is the weighted sum of  $x_1$  and  $x_2$ . There was a high agreement between the experimental data and the model calculation under different heating rates. To quantify the errors in predicting the values of fractional conversion, the experimental and calculated values were compared using *DEV* between the calculated and experimental curves using Eq. 12. The same procedure was applied to the fractional conversion curve using Eq. 13. These results are summarized in Table 5. The error of the various samples can be ranked in the order PS > BS > RL > CC, and no error was higher than 1.86%. These results further illustrate the accuracy of the kinetic model proposed in

this paper. They also show that the proposed model works better for describing the oxidative decomposition process of biomass with lower contents of alkali and alkaline-earth metal oxides catalyst.

**Table 5.** Deviation between the Experimental and Calculated Curves

Samples	DEV (dx/dt) (%)	DEV (x) (%)
PS	1.86	1.62
BS	1.79	1.46
RL	1.03	0.82
CC	0.79	0.51

## CONCLUSIONS

1. The oxidative decomposition of herbaceous and wooden residues can be represented with two successive steps. The first step corresponds to the devolatilization stage characterized by a high weight loss rate, and the second step corresponds to char oxidation characterized by a low weight loss rate.
2. The whole process can be well-described by the double-parallel-random pore model. The activation energy value of volatile oxidative decomposition was in the range of 80.7 to 133.8 kJ/mol, and that of residual char was maintained between 41.7 and 67.5 kJ/mol.
3. There was a marked compensation effect between the activation energy and the pre-exponential factor for the oxidative decomposition process with different heating rates.

## ACKNOWLEDGMENTS

This work was supported by the National Basic Research Program of China (973 Program) (2012CB720401) and the Fundamental Research Funds for the Central Universities (FRF-TP-15-063A1).

## REFERENCES CITED

- Amutio, M., Lopez, G., Aguado, R., Artetxe, M., Bilbao, J., and Olazar, M. (2012). "Kinetic study of lignocellulosic biomass oxidative pyrolysis," *Fuel* 95, 305-311. DOI: 10.1016/j.fuel.2011.10.008
- Amutio, M., Lopez, G., Alvarez, J., Moreira, R., Duarte, G., Munes, J., Olazar, M., and Bilbao, J. (2013). "Pyrolysis kinetics of forestry residues from the Portuguese Central Inland Region," *Chemical Engineering Research and Design* 91, 2682-2690. DOI: 10.1016/j.cherd.2013.05.031
- ASTM D240-02 (2007). "Heat of combustion of liquid hydrocarbon fuels by bomb calorimeter," ASTM International, West Conshohocken, USA.

- Azar, C., Lindgren, K., Larson, E., and Möllersten, K. (2006). "Carbon capture and storage from fossil fuels and biomass – Costs and potential role in stabilizing the atmosphere," *Climatic Change* 74(1), 47-79. DOI: 10.1007/s10584-005-3484-7
- Bhatia, S. K., and Perlmutter, D. D. (1980). "A random pore model for fluid-solid reactions. I. Isothermal kinetic control," *AIChE Journal* 26, 379-385.
- Ceylan, S., Topcu, Y., and Ceylan, Z. (2014). "Thermal behaviour and kinetics of alga *Polysiphonia elongata* biomass during pyrolysis," *Bioresource Technology* 171, 193-198. DOI: 10.1016/j.biortech.2014.08.064
- Chen, C. X., Ma, X. Q., and Liu, K. (2011). "Thermogravimetric analysis of microalgae combustion under different oxygen supply concentrations," *Applied Energy* 88, 3189-3196. DOI: 10.1016/j.apenergy.2011.03.003
- Cheng, K., Winter, W. T., and Stipanovic, A. J. (2012). "A modulated-TGA approach to the kinetics of lignocellulosic biomass pyrolysis/combustion," *Polymer Degradation and Stability* 97, 1606-1615. DOI: 10.1016/j.polymdegradstab.2012.06.027
- Font, A., Verdu, E., and Devesa, J. (1991). "Thermogravimetric kinetic study of the pyrolysis of almond shells and almond shells impregnated with  $\text{CoCl}_2$ ," *Journal of Analytical and Applied Pyrolysis* 21, 249-264. DOI: 10.1016/0165-2370(91)80001-O
- GB/T 212-2001 (2001). "Proximate analysis of coal," Standardization Administration of China, Beijing, China.
- GB/T 476-2001 (2001). "Ultimate analysis of coal," Standardization Administration of China, Beijing, China.
- Gil, M. V., Casal, D., Pevida, C., Pis, J. J., and Rubiera, F. (2010). "Thermal behaviour and kinetics of coal/biomass blends during co-combustion," *Bioresource Technology* 101, 5601-5608. DOI: 10.1016/j.biortech.2010.02.008
- Heikkinen, J. M., Hordijk, J. C., De Jong, W., and Spliethoff, H. (2004). "Thermogravimetry as a tool to classify waste components to be used for energy generation," *Journal of Analytical and Applied Pyrolysis* 71(2), 883-900. DOI: 10.1016/j.jaap.2003.12.001
- Huang, Y. Q., Yin, X. L., Wu, C. Z., Wang, C. W., Xie, J. J., Zhou, Z. Q., Ma, L. L., and Li, H. B. (2009). "Effect of metal catalysts on  $\text{CO}_2$  gasification reactivity of biomass char," *Biotechnology Advances* 27, 568-572. DOI: 10.1016/j.biotechadv.2009.04.013
- Hu, S. C., Ma, X. Q., Liu, Y. S., Yu, Z. S., and Fang, S. W. (2015). "Thermogravimetric analysis of the co-combustion of paper mill sludge and municipal solid waste," *Energy Conversion and Management* 99, 112-118. DOI: 10.1016/j.enconman.2015.04.026
- Jenkins, B. M., Baxter, L. L., Miles, Jr., T. R., and Miles, T. R. (1998). "Combustion properties of biomass," *Fuel Processing Technology* 54, 17-46. DOI: 10.1016/S0378-3820(97)00059-3
- Lahijani, P., Zainal, Z. A., Mohamed, A. R., and Mohammadi, M. (2013a). " $\text{CO}_2$  gasification reactivity of biomass char: Catalytic influence of alkali, alkaline earth and transition metal salts," *Bioresource Technology* 144, 288-295. DOI: 10.1016/j.biortech.2013.06.059
- Lahijani, P., Zainal, Z. A., Mohamed, A. R., and Mohammadi, M. (2013b). "Co-gasification of tire and biomass for enhancement of tire-char reactivity in  $\text{CO}_2$  gasification process," *Bioresource Technology* 138, 124-130. DOI: 10.1016/j.biortech.2013.03.179
- Lehmann, J. (2007). "A handful of carbon," *Nature* 447, 143-144. DOI: 10.1038/447143a

- Li, X. G., Ma, B. G., Xu, L., Hu, Z. W., and Wang, X. G. (2006). "Thermogravimetric analysis of the co-combustion of the blends with high ash coal and waste tyres," *Thermochimica Acta* 441, 79-83. DOI: 10.1016/j.tca.2005.11.044
- Li, X. G., Lv, Y., Ma, B. G., Jian, S. W., and Tan, H. B. (2011). "Thermogravimetric investigation on co-combustion characteristics of tobacco residue and high-ash anthracite coal," *Bioresource Technology* 102, 9783-9788. DOI: 10.1016/j.biortech.2011.07.117
- Li, X. M., Li, Y. P., Deng, Q. W., and Lin, Q. Z. (2012). "Effects of oxygen concentration in oxidizer on ignition of a biogas," *Journal of University of Science and Technology of China* 42(10), 799-806.
- Liu, X., Chen, M. Q., and Wei Y. H. (2015a). "Kinetics based on two-stage scheme for co-combustion of herbaceous biomass and bituminous coal," *Fuel* 143, 577-585. DOI: 10.1016/j.fuel.2014.11.085
- Liu, X., Chen, M. Q., and Wei, Y.H. (2015b). "Combustion behavior of corncob/bituminous coal and hard wood/bituminous coal," *Renewable Energy* 81, 355-365. DOI: 10.1016/j.renene.2015.03.021
- National Bureau of Statistics of China (NBS). (2014). *China Statistical Yearbook*, Statistic Press, Beijing, China.
- National Development and Reform Commission (NDRC). (2010). *China's 12<sup>th</sup> Five-Year Economic and Social Development Plan*, Beijing, China.
- Norgate, T., Haque, N., Somerville, M., and Jahanshahi, S. (2012). "Biomass as a source of renewable carbon for iron and steelmaking," *ISIJ International* 52(8), 1472-1481. DOI: 10.2355/isijinternational.52.1472
- Sait, H. H., Hussain, A., Salema, A. A., and Ani, F. N. (2012). "Pyrolysis and combustion kinetics of data palm biomass using thermogravimetric analysis," *Bioresource Technology* 118, 382-389. DOI: 10.1016/j.biortech.2012.04.081
- Senneca, O., Chirone, R., and Salatino, P. A. (2002). "Thermogravimetric study of nonfossil solid fuels. 2. Oxidative pyrolysis and char combustion," *Energy Fuels* 16, 661-668. DOI: 10.1021/ef0102061
- Shen, D. K., Gu, S., Luo, K. H., Bridgwater, A. V., and Fang, M. X. (2009). "Kinetic study on thermal decomposition of woods in oxidative environment," *Fuel* 88, 1024-1030. DOI: 10.1016/j.fuel.2008.10.034
- Sun, Z., Shen, J., Jin, B., and Wei, L. (2010). "Combustion characteristics of cotton stalk in FBC," *Biomass and Bioenergy* 34, 761-770. DOI: 10.1016/j.biombioe.2010.01.019
- Wang, Y. J., Bi, Y. Y., and Gao, C. Y. (2010). "The assessment and utilization of straw resource in China," *Agricultural Sciences of China* 9, 1807-1815. DOI: 10.1016/S1671-2927(09)60279-0
- Wang, C. A., Zhang, X., Liu, Y., and Che, D. (2012). "Pyrolysis and combustion characteristic of coals in oxygen fuel combustion," *Applied Energy* 97, 264-273. DOI: 10.1016/j.apenergy.2012.02.011
- Wang, S., Jiang, X. M., Wang, Q., and Ji, H. S. (2013). "Fluidized bed combustion of seaweed biomass particles," *CIESC Journal* 64(5), 1592-1599.
- Wang, G. W., Zhang, J. L., Shao, J. G., and Ren, S. (2014). "Characterisation and model fitting kinetic analysis of coal/biomass co-combustion," *Thermochimica Acta* 591, 68-74. DOI: 10.1016/j.tca.2014.07.019
- Wang, G. W., Zhang, J. L., Hou, X. M., Shao, J. G., and Geng, W. W. (2015). "Study on CO<sub>2</sub> gasification properties and kinetics of biomass chars and anthracite char," *Bioresource Technology* 177, 66-73. DOI: 10.1016/j.biortech.2014.11.063

- White, J. E., Catallo, W. J., and Legendre, B. L. (2011). "Biomass pyrolysis kinetic: A comparative critical review with relevant agricultural residue case studies," *Journal of Analytical and Applied Pyrolysis* 91, 1-33. DOI: 10.1016/j.jaap.2011.01.004
- Xu, Y. G., Zhang, C., Xia, J., Duan, Y. H., Yin, J. J., and Chen, G. (2010). "Experimental study on the comprehensive behavior of combustion for blended coals," *Asia-Pacific Journal of Chemical Engineering* 5, 435-440. DOI: 10.1002/apj.264
- Yu, Z., and Kong, X. L. (2013). "Industrial structure, carbon dioxide emission and economic growth," *Economics Management* 511, 24-33.
- Zhang, J. L., Wang, G. W., Shao, J. G., and Zuo, H. B. (2014). "A modified random pore model for the kinetics of char gasification," *BioResources* 9, 3497-3507. DOI: 10.15376/biores.9.2.3497-3507
- Zhao, J., and Wang, S. Y. (2008). "Bio-energy resource and its utilization in China," *Solar Energy* 2(1), 90-94.
- Zhu, Q., and Luo, Z. H. (2015). "China's energy structure research based on grey correlation model," *Ecological Economy* 31(4), 34-38.
- Zhu, X., Li, G., Feng, Y. P., and Liao, Q. (2006). "Thermogravimetric experiments and component analysis of biomass in Chongqing," *Journal of Chongqing University: Natural Science Edition* 29(8), 44-48.

Article submitted: December 17, 2015; Peer review completed: February 6, 2016;  
Revised version received and accepted: April 4, 2016; Published: April 14, 2016.  
DOI: 10.15376/biores.11.2.4821-4838